Available online at www.sciencedirect.com
ScienceDirect
Journal of the European Ceramic Society 30 (2010) 2661–2670
www.elsevier.com/locate/jeurceramsoc

High temperature oxidation of SiC under helium with low-pressure oxygen. Part 2: CVD β-SiC

L. Charpentier [a], M. Balat-Pichelin [a,*], H. Glénat [a], E. Bêche [a], E. Laborde [c], F. Audubert [b]

[a] *PROMES-CNRS, 7 rue du four solaire, 66120 Font-Romeu – Odeillo, France*
[b] *CEA, DEN, DEC/SPUA/LTEC, 13108 St Paul lez Durance, France*
[c] *SPCTS, Université de Limoges, 123 avenue Albert Thomas, 87060 Limoges, France*

Abstract

In the frame of the Generation IV International Forum, Gas-cooled Fast Reactor (GFR) is one system studied by CEA (France). Helium pressurized at 7 MPa is the coolant and the nominal temperature of use is about 1300 K. The cladding materials currently considered is a SiC/SiC composite with a β-SiC coating. In case of accident, reactor temperatures can reach 1900–2300 K. A previous study was carried out to determine the physico-chemical behavior of another polytype, α-SiC, for comparison on the position of the active to passive transition and of the mass loss rates under active conditions to simulate a typical accident. Experimental oxidation tests at high temperature (1400–2300 K) on massive β-SiC samples processed by Chemical Vapor Deposition (CVD) coupled to mass variation, SEM, XPS, AFM and roughness analyses enabled to determine the transition between passive and active oxidation regimes, and to study the resistance to oxidation of such material in some conditions that might be encountered in case of accident (high temperature increase up to 2300 K). Finally, the experimental results have shown that the transition from passive to active regime occurs at higher temperature for β-SiC than for α-SiC and that the mass loss rate of β-SiC is lower than the one measured for α-SiC on the common temperature range investigated (up to 2100 K).

Keywords: B. Surfaces; C. Corrosion; D. SiC; E. Nuclear applications; High temperature

1. Introduction

Increasing the efficiency of fission energy by producing energy at higher temperatures than the current second and third generation of nuclear systems implies the conception of new nuclear systems. In the frame of the Generation IV forum, the conception of new reactors requiring different safety and reliability issues than the current ones will be based on several technologies like liquid sodium, molten salts or gaseous helium coolants instead of pressurized water. In this study, the one of interest is the GFR (Gas-cooled Fast Reactor) system that features a fast-spectrum helium-coolant reactor and closed fuel cycle. The nominal working condition of this system is a temperature level about 1300 K with an elevated total pressure of 7 MPa. Such high temperatures enable not only to deliver electricity but also heat for different industrial processes (hydrogen production, reduction of metallic oxides, etc.) with high conversion efficiency. The main technological challenge is the development of the cladding materials resisting to damage at very high temperatures, fast-neutron fluences and with enhanced fission product retention capability. SiC is an excellent candidate for these requirements and nuclear fuel claddings are planned to be in high thermal conductive SiC/SiC composite with a β-SiC coating. Such coating would be able to prevent the pyrocarbon interphase present in the composite from oxidation[1,2] and to smooth the surface of the composite in order to respect the geometrical specifications.

This study focuses on the oxidation behavior of β-SiC processed by CVD under helium polluted with oxygen impurities (from 2 to 1000 ppm). The oxidation of silicon carbide specimens obeys to different mechanisms as a function of oxygen partial pressure and temperature: *passive* oxidation where a silica protective layer is formed at the surface of SiC preventing it from further oxidation, and *active* oxidation where $SiO_{(g)}$ is produced and, consequently, no protective silica layer appears whereas SiC is characterized by a significant mass loss. A previous paper[3] has reported the theoretical and experimental determination of the transition from passive to active oxidation

* Corresponding author. Tel.: +33 468 307 768; fax: +33 468 302 940.
E-mail address: marianne.balat@promes.cnrs.fr (M. Balat-Pichelin).

0955-2219/$ – see front matter © 2010 Elsevier Ltd. All rights reserved.
doi:10.1016/j.jeurceramsoc.2010.04.031

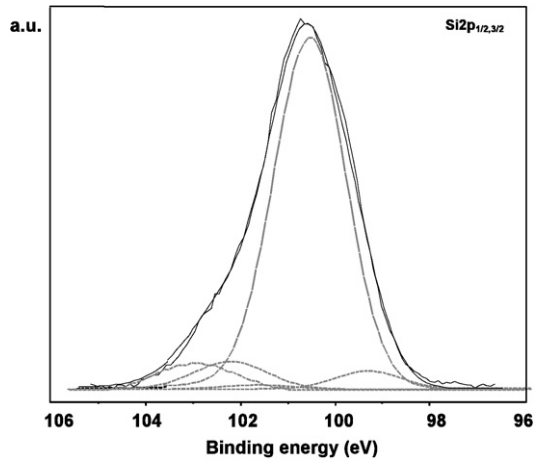

Fig. 1. Peak fitting of the Si $2p_{1/2,3/2}$ photoelectron peak obtained through XPS analysis on β-SiC before oxidation.

regime and the evolution of the material damage at high temperature for α-SiC under helium at 10^5 Pa, with oxygen partial pressure varying from 0.2 to 100 Pa, in a temperature range from 1400 to 2100 K. We have continued the investigation on the same temperature range and interval of oxygen partial pressure on β-SiC as none of the previous studies[4–7] refers to oxidation under such conditions. The aim of this study is also to compare the behavior of the two polytypes of SiC, α-SiC formerly studied[3] and β-SiC investigated here.

2. Experimental procedure

After the description of the studied material and its characterization, the oxidation procedure is presented in this section.

As we have proceeded with α-SiC, we focused on the experimental determination of the transition between passive and active oxidation and on the behavior in conditions that might be encountered in case of accident (up to 2300 K) for the β polytype using the REHPTS (REacteur Hautes Pression et Température Solaire) facility formerly described.[3] Surface characterization through Scanning Electron Microscopy (SEM), roughness measurements (mean square roughness RMS and maximal roughness variation R_{max}), Atomic Force Microscopy (AFM) and X-ray Photoelectron Spectroscopy (XPS) were used to differentiate the characteristics of passive (presence of a silica layer) or active (no silica, etched SiC surface) oxidation.

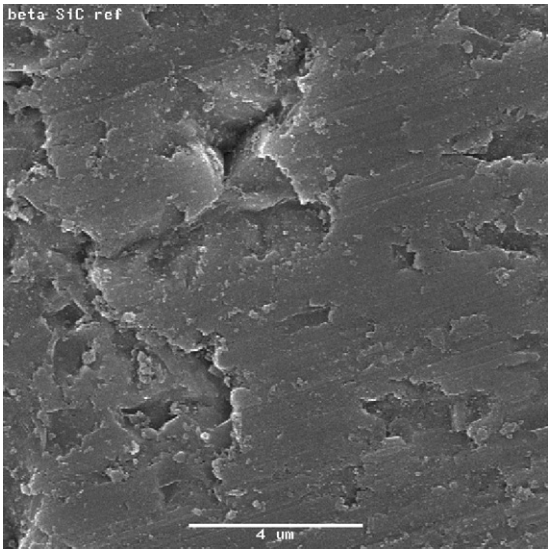

Fig. 2. SEM image of the surface of β-SiC before oxidation (the length of the scale bar is 4 μm).

2.1. Material

The silicon carbide studied is β-SiC from Rohm & Haas (USA) processed by Chemical Vapor Deposition (CVD) in a temperature range from 1470 to 1570 K. The manufacturer gives a purity of 99.9995%. The crystallographic structure is face-centered cubic and the density is close to the theoretical one (3.21). β-SiC has a higher thermal conductivity (around 300 $W\,m^{-1}\,K^{-1}$) than the α-SiC polytype (between 50 and 120 $W\,m^{-1}\,K^{-1}$) previously studied[3] and also a low coefficient of thermal expansion (CTE). The CTE of this β-SiC was measured by CEA as equal to 5.15×10^{-6} between 700 and 1500 K and the manufacturer data is 5.31×10^{-6}. The samples used in this study are squares of 25 mm and 2 mm thickness. They were polished by the manufacturer and our measurement obtained using 1D profilometry gives a mean square roughness RMS of 58 nm.

XPS analyses were performed on the samples (reference and after oxidation) using the KRATOS ULTRA set-up at SPCTS laboratory. The X-ray source is the Al Kα ray with energy $h\nu = 1486.6$ eV. The accuracy of the binding energy measurement is ±0.1 eV. The surfaces of the different samples were etched during 10 min using Ar^+ at 2 keV in order to remove the surface contamination.

Fig. 1 shows the Si $2p_{1/2,3/2}$ photoelectron peak collected for an untreated β-SiC sample (reference material). The main component located at 100.5 ± 0.1 eV is attributed to Si–C bonds (Si–C_4 chemical environments). The lower components located at 103.2 ± 0.1 eV, 102.2 ± 0.1 eV were attributed to Si–O bonds in SiO_2 and Si–O_xC_y ($x + y = 4$) compounds, respectively. The presence of the component located at 99.5 ± 0.1 eV characteristics of Si–Si bonds could be due to etching effects. Finally, the chemical composition of the material obtained by XPS is closed to the theoretical one with a ratio C/Si equal to 1.05.

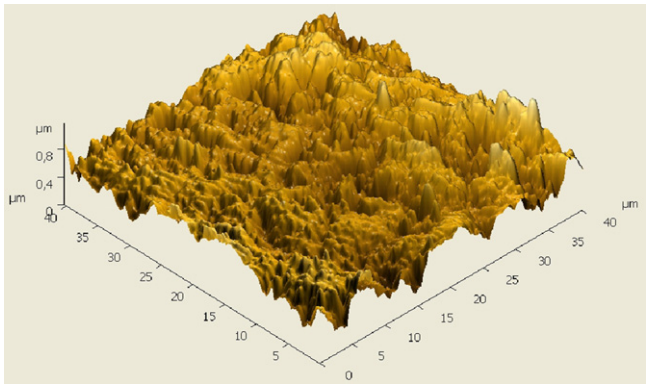

Fig. 3. AFM imaging of β-SiC before oxidation (40 μm × 40 μm).

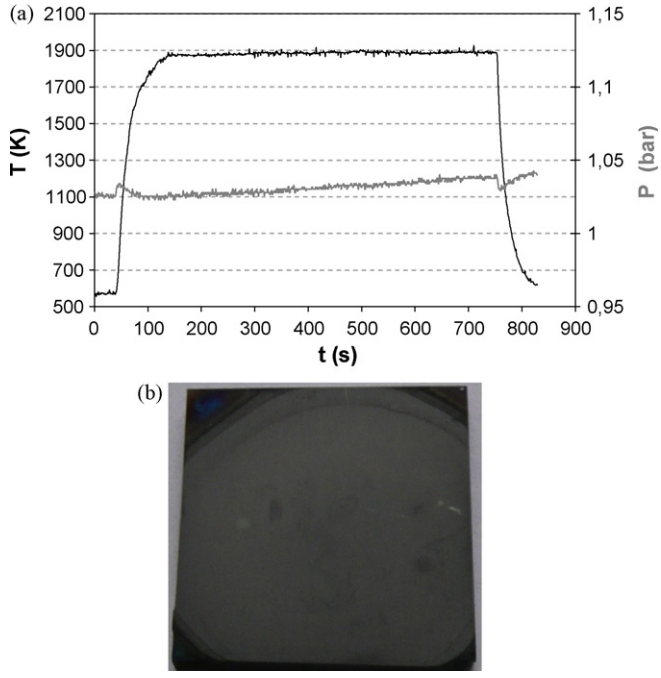

Fig. 4. (a) Typical thermal history for a sample for the determination of the oxidation regime and (b) image of an oxidized sample showing the uniformity of the solar heating.

The surface morphology of the samples was analyzed with SEM before oxidation and a typical image is presented in Fig. 2. The surface looks quite smooth with the presence of some closed porosities that is confirmed through roughness measurements and AFM imaging (Fig. 3). Indeed both techniques are complementary. Roughness measurements are performed along six 5 mm-long trajectories at different angles in order to estimate a pertinent average roughness for the analyzed sample using the profilometer Hommel Tester T2000 with a sensor Hommel Werke LV-50E. AFM imaging was performed on 40 μm × 40 μm scanned surface using a Smena MT-MDT set-up. The mean square roughness (RMS) and maximal roughness variation (R_{max}) values were measured at different scales through AFM (RMS = 153 nm, R_{max} = 1538 nm), values therefore higher than the ones measured using 1D profilometry (RMS = 58 nm, R_{max} = 472 nm) because profilometry excludes more local minima and maxima than AFM but gives roughness variations on a longer scale.

2.2. Oxidation procedure

Samples were oxidized during 10 min at constant temperature inside the REHPTS according to the same procedure previously described.[3] To reproduce the GFR atmosphere, different helium qualities from Air Liquide – 2 ppm O_2 and 3 ppm H_2O content (He Alphagaz 1) and up to 20 ppm O_2 and 5 ppm H_2O content (He U) – were used with a gas flow of 10 l min^{-1}. Pure oxygen with 2 ppm H_2O and 6 ppm N_2 (Air Liquide O_2 N48) was added to He U through a second gas line in order to increase the content of the O_2 impurity up to 1000 ppm. A safety valve with a gauge enabled us to work with a constant total pressure of 10^5 Pa under gas flow. Therefore the partial pressure of oxygen pO_2 could vary between 0.2 and 100 Pa according to the controlled oxygen content. The gas phase composition inside the reactor is checked by a mass spectrometer (©Pfeiffer Omnistar Vacuum GSD 301).

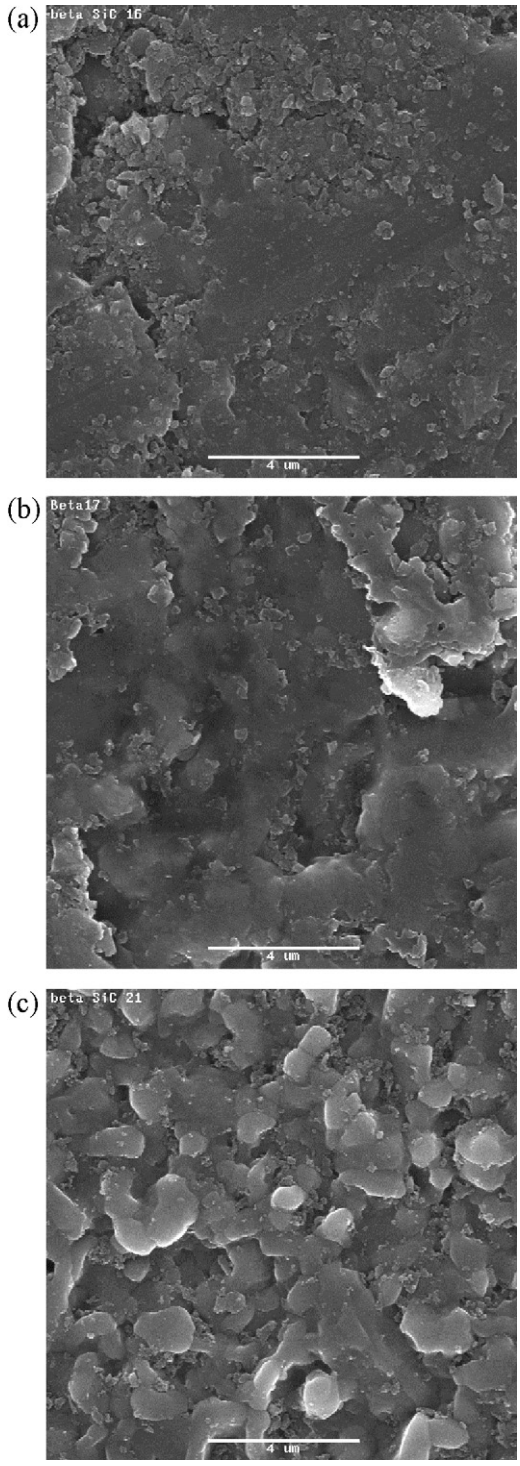

Fig. 5. SEM images of β-SiC oxidized under pO_2 = 0.2 Pa at (a) 1595 K (sample no. 16), (b) 1653 K (sample no. 17) and (c) 2120 K (sample no. 21). The length of the scale bar is 4 μm.

Two samples were pre-oxidized during 24 h at 1300 K under ambient air inside an electrical furnace before being treated inside the REHPTS above 2100 K under helium with pO_2 = 2 Pa, in order to define the effect of a silica layer on the active oxida-

tion kinetics. The mass gain measured after the thermal oxidative pre-treatment corresponds to the production of an approximately 100 nm thick silica layer on each sample.

In situ analysis of the gaseous phase was performed using the mass spectrometer enabling to follow the variation of the intensity corresponding to the gaseous species CO (at $m/e = 28$) and SiO (at $m/e = 44$).

Mass variation was measured by weighting the samples before and after oxidation, converted to percentage and rates of mass change are expressed in $mg\,cm^{-2}\,h^{-1}$. These mass variations and various surface analyses (SEM observations, roughness measurements through AFM and profilometry, XPS analyses) enabled to determine the oxidation regime (passive or active).

A monochromatic (5 μm) optical pyrometer is used to measure the surface temperature of the sample during all the experiment. At a distance of 1200 mm between the sample and the optical pyrometer, the temperature is measured on an area of 6 mm in the centre of the sample, and due to the position of the sample 25 mm above the focus, a homogeneous concentrated solar flux is obtained on the sample. The spectral normal emissivity taken for SiC is 0.90 at this wavelength and it does not change during passive or active oxidation, silica presenting the same emissivity than SiC at this wavelength. The accuracy of the temperature measurements at the surface of the β-SiC sample is going from 1400 ± 15 K to 2300 ± 25 K mainly due to the accuracy of the pyrometer. Fig. 4(a) presents a typical thermal history of a sample during oxidation with the first huge temperature increase due to the absorption of the concentrated solar radiation followed by the temperature plateau and (b) shows an image of one sample after the oxidation procedure where the result of the homogeneous solar flux is clearly visible. In Fig. 4(a), the first points around 550–600 K have not to be taken into account as our pyrometer can measure temperatures only above this level. Nevertheless, the opening of the shutter leading to the temperature increase begins at $t = 0$ s and the shutter is closed at around $t = 750$ s leading by the natural cooling of the material due to its thermal properties. The total pressure during the experiment is also shown in Fig. 4(a).

3. Experimental results

In this section are presented the surface characterization of several selected samples after oxidation according to temperature and oxygen partial pressure, the *in situ* amount of some gaseous emitted species during the oxidation process and mainly those at m/e equal to 28 and 44, the experimental determination of the transition between passive and active oxidation and finally the kinetics of active oxidation at high temperature.

3.1. Surface characterization

SEM images enable to determine the oxidation regime close to the transition under $pO_2 = 0.2$ Pa (Fig. 5), 2 Pa (Fig. 6) and

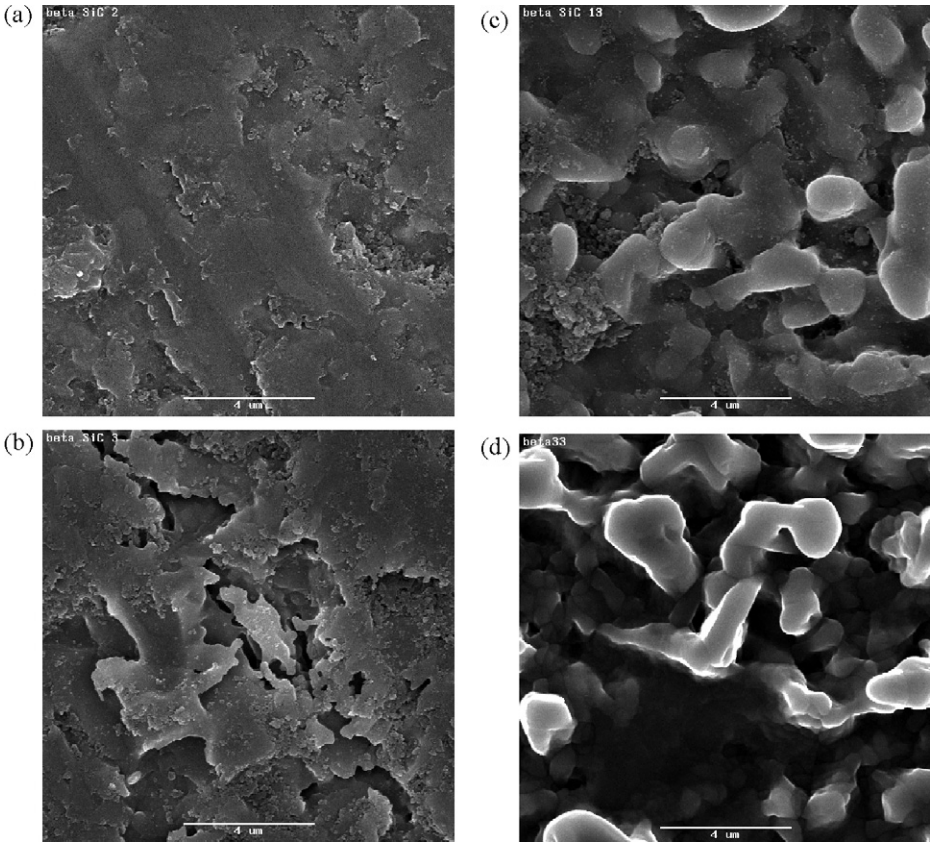

Fig. 6. SEM images of β-SiC oxidized under $pO_2 = 2$ Pa at (a) 1650 K (sample no. 2), (b) 1764 K (sample no. 3), (c) 2173 K (sample no. 13) and (d) 2270 K (sample no. 33). The length of the scale bar is 4 μm.

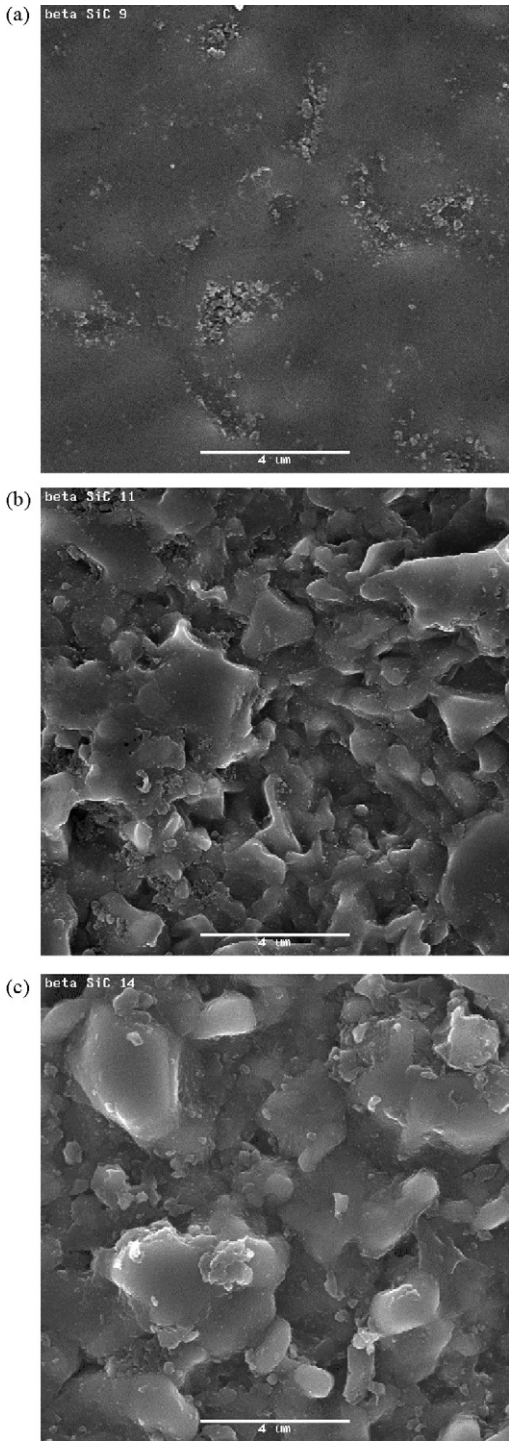

Fig. 7. SEM images of β-SiC oxidized under pO_2 = 100 Pa at (a) 1739 K (sample no. 9), (b) 1900 K (sample no. 11) and (c) 2119 K (sample no. 14). The length of the scale bar is 4 μm.

100 Pa (Fig. 7). On these figures, we observe on the (a) images the presence of a silica layer, characteristic of the passive regime and on the (b) images the presence of etched areas revealing the grains, characteristic of the active one. The higher the partial pressure is the more significant the differences are. The (c) images are obtained on samples tested under conditions that can be encountered in case of accident, respectively at 2120 K (sample no. 21, Fig. 5), 2173 K (sample no. 13, Fig. 6) and 2119 K (sample no. 14, Fig. 7). We can notice on these three figures an important development of columnar grains at such high temperature. At 2270 K and for pO_2 = 2 Pa (sample no. 33 in Fig. 6(d)), it is even more difficult to focus on both the revealed grains and the deeper etched areas. The cause of this grain development is the preferential attack that is mainly due to the different orientations of the grains, C-terminated plans being known to be more reactive to oxygen than Si-terminated plans.[8,9]

Table 1 presents the measurements of the mean square roughness RMS and of the maximal roughness variation R_{max} using profilometry for the reference sample and for oxidized samples under pO_2 = 0.2, 2 and 100 Pa, at various temperatures. Few change in the roughness values is detected for the samples oxidized under pO_2 = 0.2 Pa, the lowest partial pressure studied. Under pO_2 = 2 Pa, we can notice that the roughness of the samples oxidized under active regime increases with the temperature due to the more significant development of the grains. Under pO_2 = 100 Pa, we notice an important increase of RMS and R_{max} values close to the transition. Indeed comparing the SEM images of Figs. 5(b), 6(b) and 7(b) show that under pO_2 = 100 Pa a much more etched surface is present close to the transition than at lower oxygen partial pressure due to the more important supply of oxygen. Around 2150 K (samples no. 21, 13 and 14), we observe that the RMS and R_{max} values are on the same range under pO_2 = 0.2, 2 and 100 Pa. Under pO_2 = 100 Pa, the surface roughness is even lower at 2120 K than at 1900 K. The grains growth at such elevated temperature could explain the decrease of roughness under pO_2 = 100 Pa and the identical size of the remaining grains regardless the oxygen partial pressure.

Fig. 8 presents AFM images obtained on β-SiC oxidized under pO_2 = 2 Pa at (a) 1650 K (sample no. 2) and at (b) 2173 K (sample no. 13). Fig. 9 presents the ones obtained after oxidation under pO_2 = 100 Pa at (a) 1739 K (sample no. 9) and at (b) 2119 K (sample no. 14). The AFM revealed different morphologies between samples oxidized under passive (a) and active (b) conditions. Grain development is observed in Figs. 8(b) and 9(b) as also on SEM images (Figs. 6(c) and 7(c)). Table 2 presents the RMS and R_{max} values measured using AFM on these 4 oxidized samples. These values are on the same range for the samples no. 2 and 9 that supported passive oxidation and close to the reference values. The RMS and R_{max} values are much more important (nearly twice) for the samples no. 13 and 14 that supported active oxidation. AFM gives roughness values very close for these two samples oxidized around 2150 K but under different pO_2 (2 Pa for sample no. 13, 100 Pa for sample no. 14) confirming that the surface roughness is not affected by the oxygen partial pressure at such temperature as previously measured using profilometry.

XPS analysis (performed after 10 min Ar^+ etching) gives other information on the composition close to the surface of oxidized samples. Table 3 contains the amount of each component for the deconvoluted C 1s (Table 3a), Si $2p_{1/2,3/2}$ (Table 3b) and O 1s (Table 3c) photoelectron peaks collected for oxidized samples no. 2, 9 and 13. For example, Fig. 10 shows the results of the peak fitting procedure for the Si $2p_{1/2,3/2}$ photoelectron peak for the samples no. 2 (pO_2 = 2 Pa, 1650 K), no. 9 (pO_2 = 100 Pa, 1739 K) and no. 13 (pO_2 = 2 Pa, 2173 K). The component located

Table 1
Mean square roughness measurements RMS and maximum roughness variation R_{max} (using a 1D-profilometer) for reference β-SiC and oxidized samples under various pO_2.

Sample (temperature and oxidation regime)	Reference β-SiC	16 (1595 K, passive)	17 (1653 K, active)	21 (2120 K, active)
$pO_2 = 0.2$ Pa				
RMS (nm)	58	134	107	104
R_{max} (nm)	472	1028	958	937

Sample (temperature and oxidation regime)	Reference β-SiC	2 (1650 K, passive)	3 (1764 K, active)	13 (2173 K, active)	33 (2270 K, active)
$pO_2 = 2$ Pa					
RMS (nm)	58	75	74	114	395
R_{max} (nm)	472	705	564	805	2848

Sample (temperature and oxidation regime)	Reference β-SiC	9 (1739 K, passive)	11 (1900 K, active)	14 (2119 K, active)
$pO_2 = 100$ Pa				
RMS (nm)	58	93	267	108
R_{max} (nm)	472	1487	2400	760

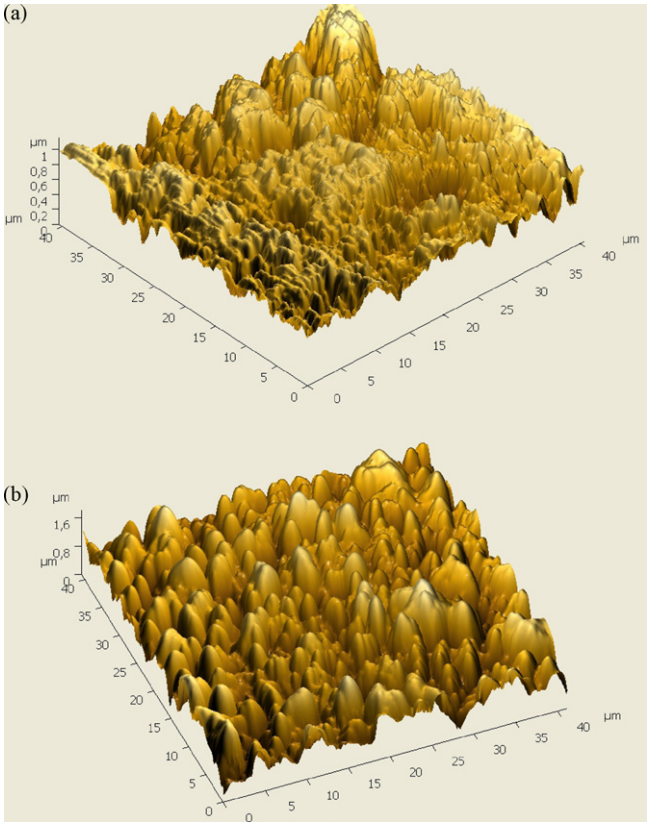

Fig. 8. AFM images of β-SiC oxidized under $pO_2 = 2$ Pa at (a) 1650 K (sample no. 2) and (b) 2173 K (sample no. 13).

Table 2
Mean square roughness measurements RMS and maximum roughness variation R_{max} (using AFM) for reference β-SiC and oxidized samples under various pO_2.

Sample	Reference	2, passive	13, active	9, passive	14, active
RMS (nm)	153	174	314	114	334
R_{max} (nm)	1538	1173	1843	1061	2026

at 100.5 ± 0.1 eV is attributed to Si–C bonds. The amount of Si–C bonds (Table 3b) and C–Si bonds (Table 3a) increases with increasing the oxidation temperature due to the presence of mainly SiC on the surface (active oxidation). The component detected at 103.2 ± 0.1 eV is attributed to Si–O bonds in SiO_2 compounds (more important in Fig. 10(a) and (b)). The amount of Si–O bonds (Table 3b) and O–Si bonds (Table 3c) decreases with increasing the oxidation temperature due to the same reason as before, samples no. 2 and 9 being under passive oxidation conditions and sample 13 under active oxidation. The three lower

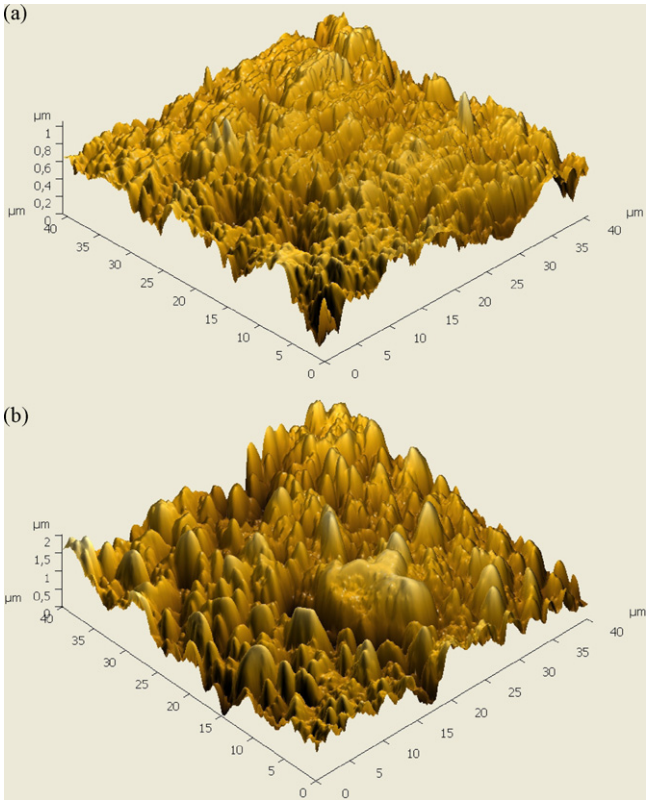

Fig. 9. AFM images of β-SiC oxidized under $pO_2 = 100$ Pa at (a) 1739 K (sample no. 9) and (b) 2119 K (sample no. 14).

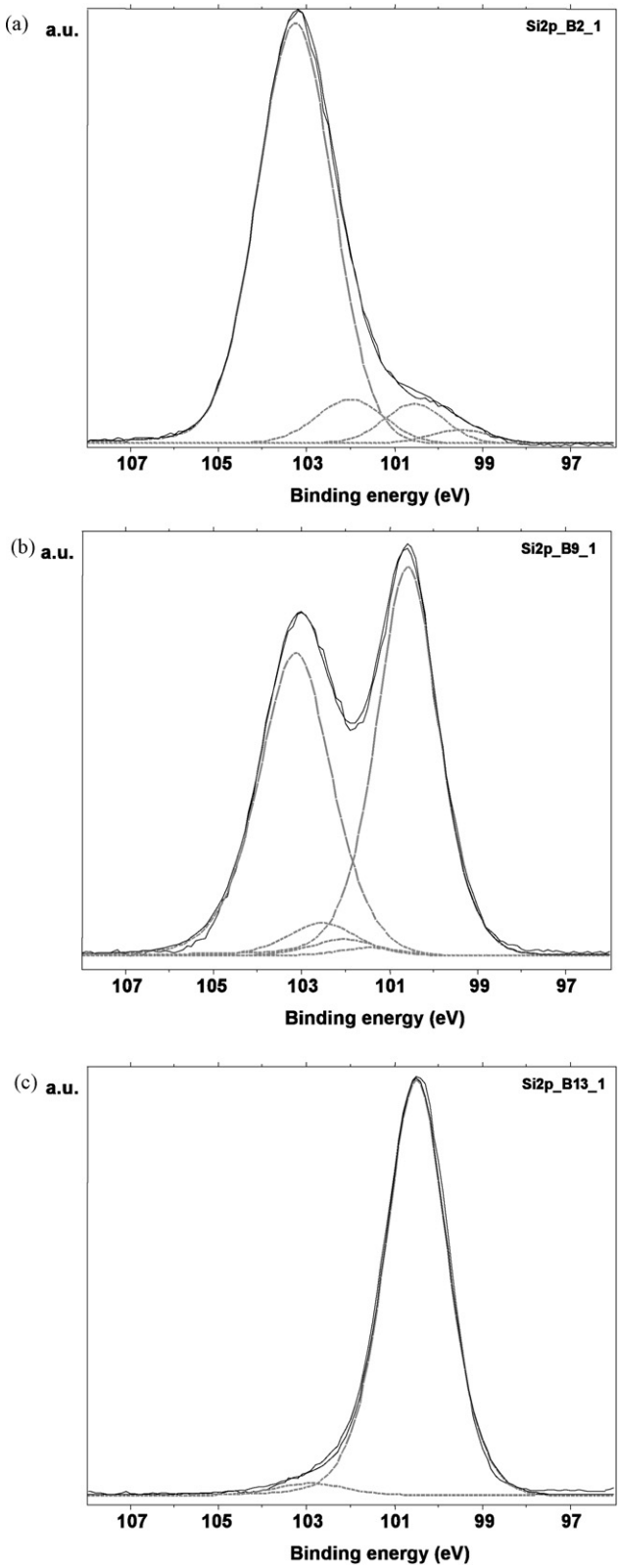

Fig. 10. Peak fitting of the Si $2p_{1/2,3/2}$ photoelectron peak obtained using XPS (after 10 min Ar^+ etching) on (a) sample no. 2 (pO_2 = 2 Pa, 1650 K), (b) sample no. 9 (pO_2 = 100 Pa, 1739 K) and (c) sample no. 13 (pO_2 = 2 Pa, 2173 K).

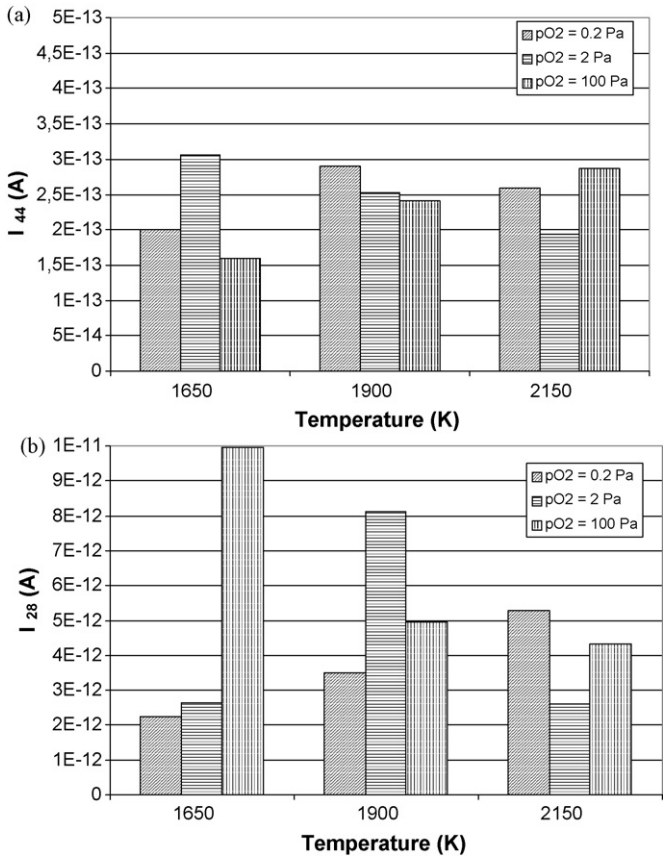

Fig. 11. Intensities measured with the mass spectrometer at various temperatures and pO_2 for the signal at (a) $m/e = 44$ and (b) $m/e = 28$.

components located at 101.4, 102.0 and 102.5 ± 0.1 eV were attributed to O–Si–C bonds in Si–O_xC_y ($x + y = 4$) compounds. The significant increase of Si–O bonds on samples no. 2 and 9 is due to the production of silica during passive oxidation whereas the bonds Si–C and C–Si are the preponderant contributions on the surface of sample no. 13 while hardly no silica was produced showing the oxidation was active. The contribution of Si–C and C–Si bonds for the sample no. 9 is more important than the contributions of those bonds for the sample no. 2 so the contribution of the SiC material is more important for the sample no. 9 than for no. 2 which might be due to a thinner or broken oxide layer.

3.2. Gaseous phase analysis

Ogura et al.[10] have reported that the condensation of the SiO at lower temperature prevents this gas from reaching the analysis chamber of a mass spectrometer, therefore such a set-up cannot be used to detect the production of SiO. Indeed, Ogura et al.[10] have determined the transition following the intensity of the signal at $m/e = 28$, corresponding to CO. They measured a more important intensity for active oxidation than for passive oxidation, as the presence of one silica layer slows down the production and the release of the CO. Fig. 11 presents the signals measured at (a) $m/e = 44$ (SiO) and at (b) $m/e = 28$ (CO) under pO_2 = 0.2, 2 and 100 Pa and at 1650, 1900 and 2150 K. The signal at $m/e = 44$ is slightly higher than the limit of detection of the spectrometer (10^{-13} A) and it does not change signifi-

Table 3
Contribution of the different chemical bonds determined using XPS (after 10 min Ar^+ etching) for the oxidized samples no. 2 (pO_2 = 2 Pa, 1650 K), no. 9 (pO_2 = 100 Pa, 1739 K) and no. 13 (pO_2 = 2 Pa, 2173 K).

β-SiC sample no.	Total C 1s	C–Si (282.6 eV)	C–C/C–H (285 eV)	C–O (286.6 eV)	C=O (288.5 eV)
(a)					
2	17.3	2.3	12.8	1.6	0.6
9	27.1	15.2	10.8	1.1	–
13	47.4	34.3	13.1	–	–
β-SiC sample no.	Total Si 2p	Si–Si (99.5 eV)	Si–C (100.5 eV)	Si–O_xC_y (102 eV)	Si–O (103.2 eV)
(b)					
2	33.9	0.7	2.1	2.7	28.4
9	39.7	–	19.6	3.1	17.0
13	44.4	–	42.0	–	2.4
β-SiC sample no.					O–Si (531.7 eV)
(c)					
2					47.7
9					32.5
13					7.1

cantly during active oxidation due to the condensation of SiO. Under pO_2 = 0.2 Pa, the transition temperature is lower than 1650 K, therefore the three temperatures correspond to active oxidation and the signal at m/e = 28 increases due to a more important CO production when the temperature increases. Under pO_2 = 2 Pa and pO_2 = 100 Pa, the oxidation is passive at 1650 K, active at 1900 and 2150 K. Nevertheless, if the signal at m/e = 28 increases when the temperature increases from 1650 to 1900 K under pO_2 = 2 Pa, it continuously decreases for pO_2 = 100 Pa. The decrease of the signal above 1900 K might be due to the condensation of the gaseous species CO and SiO. A deposit was formed on the cooled walls of the reactor at these temperatures and the analysis of this powder, recovered just after the end of the experiment, by XRD showed that the deposit was a mixture of graphite and silica. SiO and CO which were formed at the surface of the β-SiC sample by active oxidation above 1900 K could condensate at 300 K on the walls according to the reaction:

$$SiO_{(g)} + CO_{(g)} = SiO_{2(s)} + C_{(s)}.$$

This condensation prevents the mass spectrometer from detecting the total amount of CO produced during active oxidation, especially at high temperature or high oxygen partial pressure, as the amount of SiO produced is also supposed to be higher. Around 2270 K and under pO_2 = 2 Pa (sample no. 33), we noticed that the intensity of the signal at m/e = 28 was equal to 7×10^{-12} A, twice the one measured at 2150 K. Previous thermodynamical calculations with the software GEMINI[7,11] have shown that the sublimation of SiC is possible at this temperature and pO_2 ranges with gaseous Si appearing around 2300 K. As gaseous Si gets the same molar mass than CO, this increase at 2270 K might be linked to the production of both CO and Si.

Table 4
Mass variation and oxidation regime for the oxidized β-SiC samples according to temperature T and oxygen partial pressure pO_2.

No. β-SiC	pO_2 (Pa)	T (K)	Oxidation regime	$\Delta m/m_0$ (%)	Rate of mass change (mg cm^{-2} h^{-1})
18	0.2	1530	Passive	−0.007	−0.29
16	0.2	1595	Passive	−0.005	−0.19
17	0.2	1653	Active	−0.005	−0.19
19	0.2	1853	Active	−0.066	−2.56
20	0.2	1887	Active	−0.097	−3.55
21	0.2	2120	Active	− 0.303	−10.75
1	2	1560	Passive	−0.002	−0.09
2	2	1650	Passive	−0.026	−0.99
3	2	1764	Active	−0.059	−2.41
4	2	1900	Active	−0.094	−4.19
13	2	2173	Active	−0.230	−9.09
33	2	2270	Active	−0.972	−30.62
32[a]	2	2168	Active	−0.412	−14.07
31[a]	2	2282	Active	−0.756	−26.65
7	10	1632	Passive	−0.005	−0.19
10	10	1690	Passive	−0.002	−0.09
8	10	1776	Active	−0.048	−1.88
12	10	1925	Active	−0.126	−4.83
5	100	1667	Passive	+0.028	+1.06
9	100	1739	Passive	−0.002	−0.10
6	100	1815	Passive	−0.013	−0.49
11	100	1900	Active	−0.288	−10.63
15	100	2000	Active	−0.445	−15.99
14	100	2119	Active	−0.435	−16.02

[a] Samples which have been pre-oxidized during 24 h under air at 1300 K before oxidation inside the REHPTS facility.

3.3. Determination of the transition for β-SiC

Table 4 presents the different experimental results obtained according to the applied conditions (T, pO_2). During all the experiments the total pressure was close to 10^5 Pa. The sam-

Table 5
Transition temperatures T^{pa} calculated[7] and experimentally determined for α-SiC[3] and β-SiC according to the oxygen partial pressure pO_2.

pO_2 (Pa)	Theoretical T^{pa} (K)	T^{pa}, α-SiC (K)	T^{pa}, β-SiC (K)
0.2	1300	1560	1570
2	1400	1590	1650
10	1470	1610	1710
100	1600	1640	1810

ples no. 31 and 32 correspond to the samples which have been pre-oxidized during 24 h under air at 1300 K before the oxidation inside the REHPTS facility. Every sample has lost mass probably due to the consumption of free carbon present on the surface (contamination) except sample no. 5 due to the higher partial pressure of oxygen. The classification between the samples having being oxidized in passive or active conditions was made thanks to the surface characterization previously described in Section 3.1 and according to the mass loss rates.

Fig. 12 reports the theoretical transition we calculated in a former study[3,7] using thermodynamical calculations with the GEMINI code[11] and the Wagner modified model[4,12], the experimental passive to active transition previously determined for α-SiC[3] (transition a) and the experimental transition determined here for β-SiC (transition b) using the plotted experimental data. The filled diamond points represent the samples that have supported passive oxidation and the open diamond points the samples that have supported active oxidation. Table 5 reports the theoretical and experimentally determined transition temperatures for α-SiC and β-SiC according to pO_2. The experimental transition temperature for both SiC is quite close at $pO_2 = 0.2$ Pa, then the difference increases with pO_2 and β-SiC supports passive oxidation at higher temperature than α-SiC on the investigated range of oxygen partial pressure (difference of 170 K for $pO_2 = 100$ Pa). Therefore the activation energy and pre-exponential coefficient obtained using an Arrhenius fit for β-SiC ($E_a = 670$ kJ/mol; $A = 2 \times 10^{21}$ Pa) are much lower than for α-SiC ($E_a = 1540$ kJ/mol; $A = 7 \times 10^{50}$ Pa) and closer to the theoretical values ($E_a = 360$ kJ/mol; $A = 5 \times 10^{13}$ Pa).

3.4. Kinetics of the active oxidation

Fig. 13 presents the evolution of the mass loss rates for β-SiC according to temperature and oxygen partial pressure and gives a clear vision of the impact of temperature on the mass loss rate. It increases with temperature following linear trends up to nearly 2150 K. On this temperature range, the oxygen partial pressure has no significant effect from 0.2 to 10 Pa, the mass loss rate being much more significant at $pO_2 = 100$ Pa as observed also for α-SiC.[3] Therefore we only studied the material damage at higher temperatures for $pO_2 = 2$ Pa. An acceleration of the mass loss rate was observed between 2150 and 2300 K. This acceleration could be due to the sublimation of the SiC that can occur according to the thermodynamical calculations[3,7] above this temperature with the formation of Si, SiC_2 and Si_2C. The linear trends in the temperature range that have been determined are the following ones with the corresponding correlation coefficient:

At $pO_2 = 0.2$ Pa	$v = 0.0230\ T - 38.8$	for $1650 \le T \le 2120$ K	($R^2 = 0.93$)
At $pO_2 = 2$ Pa	$v = 0.0196\ T - 31.4$	for $1650 \le T \le 2170$ K	($R^2 = 0.88$)
	$v = 0.1572\ T - 329.3$	for $2170 \le T < 2300$ K	($R^2 = 0.89$)
At $pO_2 = 10$ Pa	$v = 0.0201\ T - 33.9$	for $1690 \le T \le 1925$ K	($R^2 = 1$)
At $pO_2 = 100$ Pa	$v = 0.0491\ T - 85.3$	for $1740 \le T \le 2120$ K	($R^2 = 0.86$)

The mass loss rates for β-SiC are lower than the ones previously measured for α-SiC at temperatures up to 2100 K.[3] As an example, under $pO_2 = 100$ Pa and at 2100 K, the mass loss rate value is equal to 16 mg cm^{-2} h^{-1} for β-SiC against 23 mg cm^{-2} h^{-1} for α-SiC equivalent to a decrease of 30%. The maximal mass loss rate for β-SiC is obtained at 2270 K under $pO_2 = 2$ Pa with a mean value of 30 mg cm^{-2} h^{-1}.

The pre-oxidized samples no. 31 (2282 K) and 32 (2168 K), oxidized under $pO_2 = 2$ Pa, with a protective silica layer obtained under air at 1300 K during 24 h of about 100 nm thickness, have presented nearly the same mass loss rate than the ones without

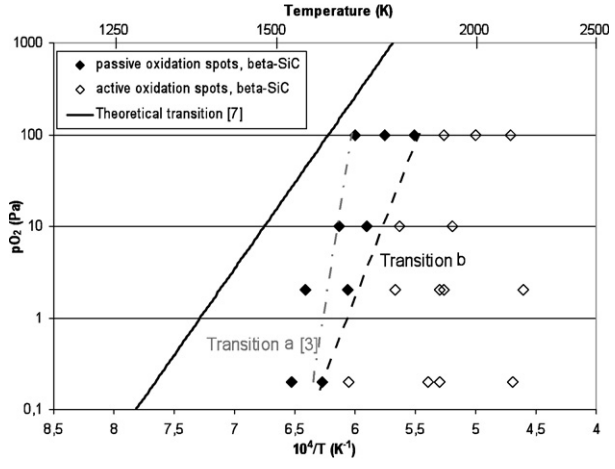

Fig. 12. Theoretical and experimental transitions between passive and active oxidation for α-SiC (transition a) and for β-SiC (transition b) using an Arrhenius plot. The points are only related to the oxidation experiments for the determination of the transition for β-SiC (open diamonds: samples under active oxidation; black filled diamonds: samples under passive oxidation).

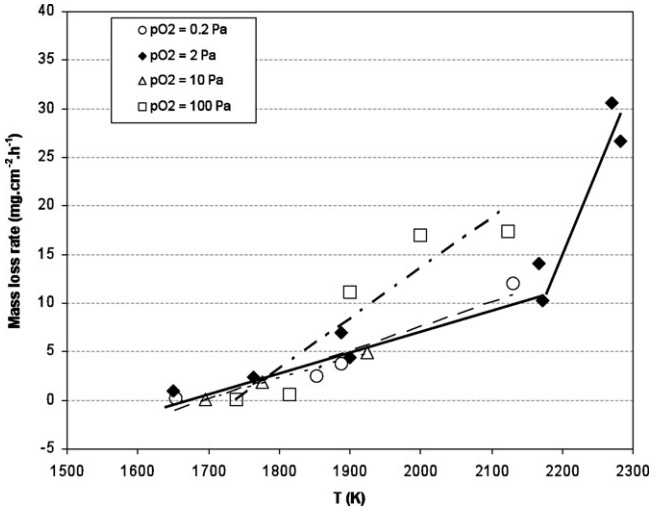

Fig. 13. Mass loss rates (mg cm^{-2} h^{-1}) of oxidized β-SiC versus temperature under active conditions for various pO_2.

silica layer at the beginning of the oxidation process (Table 4). The sublimation of this silica layer seems to follow a very quick kinetics and its presence or not has no significant effect on the final mass loss rate. More tests have to be performed with silica layers with higher thickness.

4. Conclusions

This study was done to understand the behavior of β-SiC under helium with low oxygen partial pressure and in a high temperature range of interest for GFR applications. We have determined the experimental transition law (Arrhenius fit) between passive and active oxidation for oxygen partial pressures from 0.2 to 100 Pa under a helium total pressure of 10^5 Pa and we have studied the variation of the β-SiC mass loss rates according to temperature and oxygen partial pressure under conditions that might be encountered in case of accident (up to 2300 K).

SEM, AFM imaging and XPS analyses enabled to observe significant differences between the surfaces that supported passive or active oxidation. 1D-profilometry put in evidence the more important damage of the material surface when the temperature increases above 2100 K. The following of gas production (SiO, CO) using mass spectrometry has appeared to be difficult due to the condensation of silica and graphite on the cold walls of the reactor. Nevertheless, an increase in the production of CO can be observed for the lower oxygen partial pressure and mainly close to the transition.

The temperature and oxygen partial pressure values experimentally obtained for the transition between passive and active oxidation for β-SiC are respectively equal to 1570 K at 0.2 Pa, 1650 K at 2 Pa, 1710 K at 10 Pa and 1810 K at 100 Pa. In this condition whatever the purity of helium, the nominal working temperature of the GFR (1300 K) is always lower than the transition temperature measured. Moreover, the transition between passive and active oxidation regime occurs at higher temperature for β-SiC than for α-SiC and the mass loss rate of β-SiC is lower than the one measured for α-SiC on the common temperature range investigated (up to 2100 K). Oxygen partial pressure has no significant effect on the mass loss rate in active oxidation conditions up to $pO_2 = 10$ Pa in this temperature range on the contrary to the α-SiC polytype. So high purity helium is not required to prevent β-SiC from severe active oxidation up to 2100 K in the GFR reactor. Nevertheless we observed quite an important damage of β-SiC around 2270 K under $pO_2 = 2$ Pa due to the combined phenomena of active oxidation and SiC sublimation. Therefore the mass loss rate can reach 30 mg cm^{-2} h^{-1} in such temperature area.

Acknowledgements

The authors thank the research groups MATINEX and GEDEPEON for their financial support and CEA for the funding of the post-doctoral position of L. Charpentier.

References

1. Wu S, Cheng L, Zhang L, Xu Y, Zhang Q. Comparison of oxidation behaviors of 3D C/PyC/SiC and SiC/PyC/SiC composites in an O_2–Ar atmosphere. *Mater Sci Eng B* 2006;**130**:215–9.
2. Lamouroux F, Camus G, Thébault J. Kinetics and mechanisms of oxidation of 2D woven C/SiC composites. I. Experimental approach. *J Am Ceram Soc* 1994;**77**:2049–57.
3. Charpentier L, Balat-Pichelin M, Audubert F. High temperature oxidation of SiC under helium with low-pressure oxygen. Part 1. Sintered α-SiC. *J Eur Ceram Soc* 2010;**30**:2653–60.
4. Balat MJH. Determination of the active-to-passive transition in the oxidation of silicon carbide in standard and microwave-excited air. *J Eur Ceram Soc* 1996;**16**:55–62.
5. Vaughn WL, Maahs HG. Active-to-passive transition in the oxidation of silicon carbide and silicon nitride in air. *J Am Ceram Soc* 1990;**73**:1540–3.
6. Hinze JW, Graham HC. The active oxidation of silicon and silicon carbide in the viscous gas flow regime. *J Electrochem Soc* 1976;**123**:1066–73.
7. Eck J, Balat-Pichelin M, Charpentier L, Bêche E, Audubert F. Behavior of SiC at high temperature under helium with low oxygen partial pressure. *J Eur Ceram Soc* 2008;**28**:2995–3004.
8. Song Y, Dhar S, Feldman LC, Chung G, Williams JR. Modified deal grove model for the thermal oxidation of silicon carbide. *J Appl Phys* 2004;**95**:4953–7.
9. Ramberg CE, Cruciani G, Spear KE, Tressler RE. Passive-oxidation kinetics of high-purity silicon carbide from 800 to 1100 °C. *J Am Ceram Soc* 1996;**79**:2897–911.
10. Ogura Y, Morimoto T. Mass spectrometric study of oxidation of SiC in low-pressure oxygen. *J Electrochem Soc* 2002;**149**:J47–52.
11. Thermodata, 38400 Saint Martin d'Hères, France.
12. Wagner C. Passivity during the oxidation of silicon at elevated temperature. *J Appl Phys* 1958;**29**:1295–7.